POLITECNICO DI TORINO
Repository ISTITUZIONALE

Application of Model Predictive Control in Physical Human-Machine Interaction

Original
Application of Model Predictive Control in Physical Human-Machine Interaction / Paterna, Maria; Pacheco Quiñones, Daniel; De Benedictis, Carlo; Maffiodo, Daniela; Franco, Walter; Ferraresi, Carlo. - ELETTRONICO. - 120:(2022), pp. 571-579. (Intervento presentato al convegno International Conference on Robotics in Alpe-Adria Danube Region 2022 tenutosi a Klagenfurt (Austria) nel 08/06/2022 - 10/06/2022) [10.1007/978-3-031-04870-8_67].

Availability:
This version is available at: 11583/2967214 since: 2023-10-04T09:22:05Z

Publisher:
Springer

Published
DOI:10.1007/978-3-031-04870-8_67

Terms of use:

This article is made available under terms and conditions as specified in the corresponding bibliographic description in the repository

Publisher copyright
Springer postprint/Author's Accepted Manuscript (book chapters)

This is a post-peer-review, pre-copyedit version of a book chapter published in Advances in Service and Industrial Robotics. RAAD 2022.. The final authenticated version is available online at: http://dx.doi.org/10.1007/978-3-031-04870-8_67

(Article begins on next page)

25 February 2024

POLITECNICO DI TORINO
Repository ISTITUZIONALE

Application of Model Predictive Control in Physical Human-Machine Interaction

Original
Application of Model Predictive Control in Physical Human-Machine Interaction /Paterna,Maria;Pacheco Gutiérrez, Daniel;Benedictis,Carlo;Maffiodo,Daniela;Franco,Walter;Ferraresi,Carlo. - ELETTRONICO - 12(2022), pp. 57-59. (Intervento presentato al convegno International Conference on Robotics in Alpe-Adria Danube Region 2022 tenutosi a Klagenfurt (Austria) nel 2022 - 2022) [10.1007/978-3-031-04870-6_7]

Availability:
This version is available at: 11583/2974314 since: 2023-10-04T12:22:57Z

Publisher:
Springer

Published
DOI:10.1007/978-3-031-04870-6_7

Terms of use:

This article is made available under terms and conditions as specified in the corresponding bibliographic description in the repository

Publisher copyright
Springer postprint/Author's Accepted Manuscript (bookchapters)

This is a post-peer-review,pre-copyedit version of a bookchapter published in Advances in Service and Industrial Robotics. RAAD 2022.. The final authenticated version is available online at: http://dx.doi.org/10.1007/978-3-031-04870-6_7

(Article begins on next page)

25 February 2024

solution to overcome uncertainty and disturbance factors involving test environment, versatility, and fallibility.

Previous work from the authors [11] showed how the MPC strategy could manage complex HMi interfacing issues on a hand-held mechatronic device named automatic perturbator, designed to provide, through a linear electric actuator, a controlled pushing force to the upper body of a patient in clinical postural analyses. In such environment, the contact force must be properly controlled both in terms of amplitude, to avoid overshoot potentially dangerous for the patient, and duration, to minimize postural adaptation. Based on preliminary experiments [12,13] the force impulse (i.e., the time integral of the force signal) of the applied perturbation should be comprised between 2 Ns and 10 Ns, while the duration of the stimulus should be less than 300 ms, or even less than the latency of the postural reflex (about 75-100 ms) for specific analyses. Pacheco Quiñones et al. [11] implemented a mixed speed-force control, that switched between the two references depending on the detection of the contact and on the desired motion pattern of the rod. Although the dynamics of the system was considered appropriate for the preliminary testing application, the switching behavior negatively affected the MPC strategy, due to high nonlinearities involved, and resulted in a loss of tracking accuracy.

This paper presents a renewed design based on MPC for the control of impulsive mechanical interactions directed to the human body. The hardware architecture of an automatic perturbation device is briefly presented, then the control system and its optimization are carried out by performing experimental analyses with a prototype of the perturbator. Finally, the device flexibility and robustness are also evaluated.

2 Model Predictive Control design

To fulfill the project specifications, the automatic perturbator (AP) is conceived to be operated in a hand-held arrangement as shown in Fig. 1 and Fig. 2.

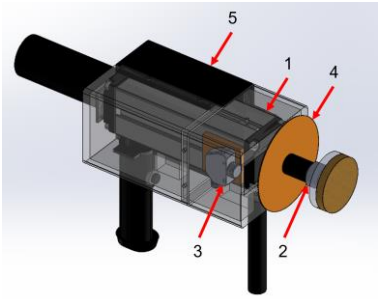

Fig. 1 CAD model of the automatic perturbator.

Table 1 List of automatic perturbator components.

N°	Component
1	GD160Q motor (NiLAB GmbH)
2	UMM 50 kgf-ranged load cell (Dacell Co. Ltd.)
3	Q4XTULAF400-Q8 optical sensor (Banner Engineering Corp.)
4	Optical sensor target disk
5	3D-printed chassis

Referring to Fig. 1 and Table 1, a 3D-printed chassis (5) surrounds a linear electric motor (1), provided with an embedded encoder and controlled through a SLVD1N driver (Parker Hannifin Corp.) and a Baseline Real-Time target machine (Speedgoat Inc.). A load cell (2) senses the impulsive force during contact, while an optical sensor (3) monitors the piston stroke through the aid of a 3D-printed target disk (4) and

manages limit-switch control. Simulink® environment (The MathWorks Inc.) is used to design the control architecture of the system and to interact with the driver's software, MotionWiz (Parker Hannifin Corp.). The device's control logic is based on the Finite State Machine (FSM) design, involving the following fundamental phases:

1. idle: in which the actuator's road is retracted, still, and ready for operation;
2. approach: button-triggered, the rod approaches the target body (Fig. 2*a*);
3. strike: the rod imparts on the target body the predefined impulsive force. The switch to this phase only occurs if the load cell output exceeds 3 N (Fig. 2*b*);
4. retraction: the rod pulls back from the target (Fig. 2*c*).

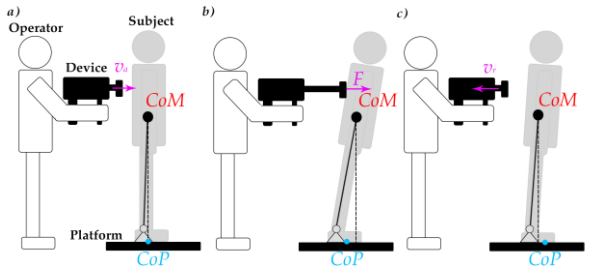

Fig. 2 Perturbator-subject interaction during approach (a), strike (b), and retraction (c) phases. CoM is the subject's center of mass, CoP is the center of pressure on the platform. In magenta, the control input signals: F is the impulsive force applied on the subject's body; v_a and v_r are, respectively, the piston approach and retraction velocities of the piston.

The operating mode of the driver's software, shown in Fig. 3, features the following elements:

- a closed-loop speed control system, based on a PI controller, working with the main driver's analog input as speed reference and using the motor's embedded encoder for feedback;
- a force reference generator, working as an alternative to the speed controller with the same main analog input, translating the voltage signal into force;
- a pico-PLC code, responsible to control the driver's software architecture during online operation;
- a current (i.e., force) saturation block, imposing the actuation current to be subjected to a saturation value equal to the minimum value among the following: peak current during normal operation; nominal current during i^2t protection; a custom constant value; an auxiliary analog input signal.

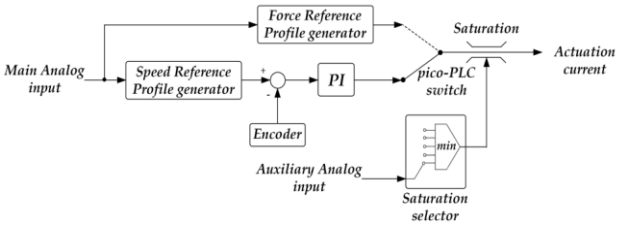

Fig. 3 Scheme of the driver's operating mode.

The presented control system focuses on the auxiliary analog input entering the saturation block (Fig. 3) to control the contact force entity. The actuator is continuously motion-controlled with a speed reference acting as the main analog input of the driver, while the auxiliary input is used to saturate the output force to achieve the desired behavior. During phases 1, 2, and 4, the force saturation is set high enough to not interfere with the inertia of the piston while, in phase 3, the current saturation is modulated by the MPC action, and the speed reference is appropriately increased to achieve the desired saturated force as fast as possible. While phases 2 and 4 can take advantage of the PI closed-loop speed control, the control of force saturation during impact implements a derived architecture of the linear MPC block used in Pacheco Quiñones et al. [11], considering a linearized lumped-parameter model of the system to reproduce the interaction shown in Fig. 2 between the operator, the AP, and the subject. The operator and the subject are modeled as lumped masses which translate in the anterior-posterior direction and connected to the environment through springs and dampers; a viscoelastic behavior is also associated to the mechanical AP-subject interface. The MPC block, thanks to the force signal provided by the load cell and the a-priori knowledge of the plant coming from the model, is able to compute an optimized step-by-step solution, predicting the system's behavior and adjusting the auxiliary input accordingly. The MPC bases its optimization on the minimization of the cost function J described in Eq. (1):

$$J(U(k|k)) = \sum_{i=0}^{H_p-1} e_y^T(k+i|k)Qe_y(k+i|k)+e_u^T(k+i|k)R_u e_u(k+i|k)+du^T(k+i|k)R_{du}du(k+i|k)+\rho_\varepsilon \varepsilon_k^2 \quad (1)$$

in which: "i|j" means that the prediction of the i^{th} time step is computed during the j^{th} time step ($j<i$); H_p is the prediction horizon, i.e., the number of future control steps that the MPC controller must evaluate by prediction; $e_{y,}$ $e_{u,}$ are the predicted error of the output and input variables, respectively, and du is the control input rate; while Q, R_u, R_{du} are their respective weight matrices. Finally, $\rho_\varepsilon \varepsilon_k^2$ is the constraint violation cost function. U(k|k) is the input macro vector, further details are given in Pacheco Quiñones et al. [11]. The force constraints of the actuation system depend on the application, i.e., the MPC controller behavior is saturated to u_{max} = 52 N (maximum force allowable), during a tunable Saturation time interval (Sdt) happening at the beginning of phase 3.

3 Experimental trials and control logic optimization

Experimental tests are designed to optimize the performance of the AP control logic. The analysis focuses on the MPC cost function, the operator stiffness (k_a) within the model, and the Sdt parameter, that are adjusted through a trial-and-error optimization process. In these tests, a rectangular pulse with an amplitude of 40 N and a duration of 250 ms is selected as the reference force signal, and the AP is handled by one operator and used to hit a rigid, fixed target. For each parameter configuration, 6 distinct stimuli are delivered.

To evaluate the device's ability to follow the desired force profile, the Tracking Accuracy Error (TAE) (Eq. (2)) and the force impulse deviation (FID) (Eq. (3)) are calculated over the time interval in which the contact force is higher than 3 N:

$$\mathrm{TAE} = 100 \cdot \frac{\int_{\Delta t} |\text{measured force} - \text{reference force}|}{\text{reference impulse value}}, \quad \Delta t = \text{contact time interval} \tag{2}$$

$$\mathrm{FID} = 100 \cdot \frac{\text{measured impulse value} - \text{reference impulse value}}{\text{reference impulse value}} \tag{3}$$

The force profiles obtained by varying R_u, Q, H_p, k_a, and Sdt are shown in Fig. 4 and Table 2, while R_{du} is kept constant and equal to 10. As R_u increases, the contact force oscillates around a lower mean value; decreasing Q causes a decrease in the amplitude and frequency of the force oscillations; despite the controller based its computation on a simplified model, increasing its power of prediction H_p from 10 to 20 steps allowed it to obtain better performance. For even higher Hp values, the system fails to calculate the optimal solution in real-time due to the high computational cost. Increasing k_a reduces ringing and allows for more stable force profiles. Sdt higher than 0 is necessary to compensate for the nonlinearities involved in the impact phase, which are not modeled in the plant due to the unknown deformation of the patient's body tissues. Sdt should be properly set and adapted to the magnitude of the reference force value to reduce the initial overshoot by maintaining a limited rising time (17.5 ± 5.3 ms). The final configuration of the parameters (*k* profile) highlights good performance: the contact force is almost constant and close to the reference throughout the considered time interval. Moreover, FID and TAE are less than 5% and 15%, respectively.

Table 2 Control parameters tuning. Mean ± standard deviation are given for force impulse (FI), force impulse deviation (FID) and tracking accuracy error (TAE). Data refer to the curves shown in Fig. 4, that have been labeled accordingly.

Profile	R_u	Q	H_p	k_a (N/m)	Sdt (ms)	FI (Ns)	FID (%)	TAE (%)
a	0.2	5	10	1600	30	9.29 ± 0.44	-7.11 ± 4.44	22.3 ± 2.66
b	0.5	5	10	1600	30	8.80 ± 0.45	-12.0 ± 4.52	21.8 ± 1.40
c	1	5	10	1600	30	7.71 ± 0.41	-22.9 ± 4.12	28.4 ± 3.81
d	0.2	2	10	1600	30	9.52 ± 0.49	-4.76 ± 4.89	18.2 ± 1.04
e	0.2	3	10	1600	30	9.61 ± 0.27	-3.91 ± 2.68	17.6 ± 1.40
f	0.2	3	15	1600	30	10.5 ± 0.92	5.06 ± 9.19	20.9 ± 4.27
g	0.2	3	20	1600	30	10.4 ± 0.18	3.60 ± 1.76	17.7 ± 1.58
h	0.2	3	20	3000	30	11.5 ± 0.49	14.7 ± 4.91	21.9 ± 4.21
i	0.2	3	20	15000	30	10.7 ± 0.44	6.98 ± 4.45	18.5 ± 1.80
j	0.2	3	20	15000	0	9.43 ± 0.50	-5.72 ± 4.97	14.5 ± 2.77
k	0.2	3	20	15000	15	10.4 ± 0.56	3.68 ± 5.61	13.6 ± 2.30

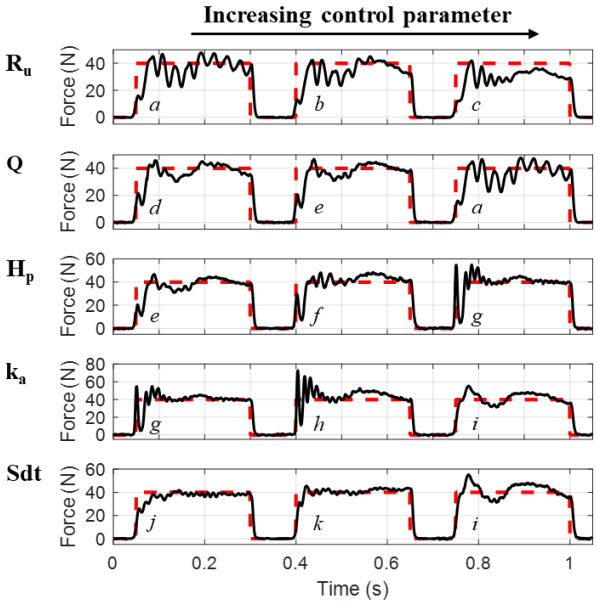

Fig. 4 Force tracking of the model predictive control algorithm for different value of R_u (control input rate), Q (tracking error), H_p (tracking error), k_a (simulated stiffness operator) and Sdt (saturation time interval). Each row of the plot refers to a specific control parameter, that has been increased from left to right side. The red dashed lines represent the reference force signal, while the averaged contact force signals are shown in black and are labeled as reported in Table 2.

The AP flexibility and robustness are evaluated by providing perturbations at different magnitudes (20, 30, 40, 50 N) in two series, carried out by two distinct operators, on a fixed target and on a healthy young subject, respectively. The results presented in Fig. 5 and Table 3 show that the tracking accuracy is not affected either by the mechanical impedance of the subject or by that of the operator. Only slight differences in fact are noticeable among the force profiles applied on a rigid, fixed target (Fig. 5, left-top) and on a human (Fig. 5, left-bottom), regardless of the force amplitude. This result supports the robustness of the device and of the control logic detailed in the current work. Moreover, as highlighted in Fig. 5, on the right, the produced force profiles show a reasonable degree of repeatability despite the variability introduced by the interaction between the AP and both the operator and the subject. The repeatability is confirmed by a FI coefficient of variation equal to 2.51%, on average.

In comparison with the previous software architecture outlined in Pacheco Quiñones et al. [11], or other analyzed devices, such as in Paterna et al. [13], the proposed control algorithm configuration shows substantial dynamic performance improvements. TAE, overshoot, and rise time of the force profiles obtained in Paterna et al. [13], in Pacheco Quinones et al. [11], and in the current work are respectively: [21.4; 24.9; 15.7] %, [44.5; 21.8; 22.6] % and [23.4; 25.4; 18.0] ms.

Table 3 Automatic perturbator performance for different force amplitudes and targets. Mean ± standard deviation are given for force impulse (FI), force impulse deviation (FID) and tracking accuracy error (TAE). Data refer to the corresponding curves shown in Fig. 5.

Force (N)	Target	Sdt (ms)	FI (Ns)	FID (%)	TAE (%)
20	fixed	0	5.49 ± 0.38	9.81 ± 7.57	17.8 ± 3.73
30	fixed	0	7.34 ± 0.35	-2.08 ± 4.67	13.9 ± 2.09
40	fixed	15	10.4 ± 0.56	3.68 ± 5.61	13.6 ± 2.30
50	fixed	20	12.8 ± 0.28	2.36 ± 2.28	11.5 ± 1.73
20	subject	0	4.94 ± 0.18	-1.20 ± 3.69	17.5 ±1.65
30	subject	0	6.90 ± 0.24	-7.94 ± 3.22	18.1 ± 2.22
40	subject	15	9.63 ± 0.08	-3.66 ± 0.82	15.7 ± 0.63
50	subject	30	11.5 ± 0.22	-7.61 ± 1.80	15.1 ± 2.45

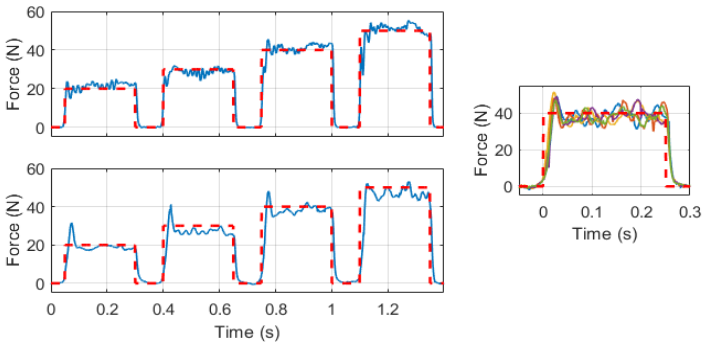

Fig. 5 Perturbation applied on a fixed target (top, left) and on a healthy subject (bottom, left) by two different operators. The red dashed lines represent the reference force profile, while the actual contact force, averaged over 6 successive stimuli, is in blue. On the right, six consecutive force signals obtained on the subject for the 40 N amplitude are shown.

4 Conclusion

The effectiveness of MPC algorithm in the control of impulsive mechanical interactions occurring between an electromechanical device and the human body has been demonstrated. The architecture of the device has been outlined and its accuracy, robustness and flexibility have been proved.

The automatic perturbator can be successfully employed in clinical dynamic posturography analysis, in which an unpredictable, short-lasting, controlled perturbation must be generated to challenge the patient's balance. However, further testing is needed to assess the robustness of the control system in a wider scenario, considering different subjects, and operators.

References

1. Ronzoni, M., Accorsi, R., Botti, L., Manzini, R.: A support-design framework for

Cooperative Robots systems in labor-intensive manufacturing processes. J. Manuf. Syst. 61, 646–657 (2021). https://doi.org/10.1016/j.jmsy.2021.10.008
2. Park, K., Lee, H., Kim, Y., Bien, Z.Z.: A Steward Robot for Human-Frindly Human-Machine Interaction in a Smart House Environment. IEEE Trans. Autom. Sci. Eng. 5, 21–25 (2008). https://doi.org/10.1109/TASE.2007.911674.
3. Kyrarini, M., Lygerakis, F., Rajavenkatanarayanan, A., Sevastopoulos, C., Nambiappan, H.R., Chaitanya, K.K., Babu, A.R., Mathew, J., Makedon, F.: A Survey of Robots in Healthcare. Technologies. 9, 8 (2021). https://doi.org/10.3390/technologies9010008
4. Guang, H., Ji, L., Shi, Y., Misgeld, B.J.E.: Dynamic modeling and interactive performance of ParM: A parallel upper-limb rehabilitation robot using impedance control for patients after stroke. J. Healthc. Eng. 2018, Article ID 8647591 (2018). https://doi.org/10.1155/2018/8647591
5. Clement, P., Veledar, O., Könczöl, C., Danzinger, H., Posch, M., Eichberger, A., Macher, G.: Enhancing Acceptance and Trust in Automated Driving trough Virtual Experience on a Driving Simulator. Energies. 15(3), 781 (2022). https://doi.org/10.3390/en15030781
6. Bower, C., Taheri, H., Wolbrecht, E.: Adaptive control with state-dependent modeling of patient impairment for robotic movement therapy. In: 2013 IEEE International Conference on Rehabilitation Robotics (ICORR). pp. 1–6. IEEE, Seattle, Washington, USA (2013). https://doi.org/doi: 10.1109/ICORR.2013.6650460.
7. Krüger, J., Surdilovic, D.: Robust control of force-coupled human-robot-interaction in assembly processes. CIRP Ann. 57, 41–44 (2008). https://doi.org/10.1016/j.cirp.2008.03.005
8. dos Santos, W.M., Siqueira, A.A.G.: Optimal impedance via model predictive control for robot-aided rehabilitation. Control Eng. Pract. 93, 104177 (2019). https://doi.org/10.1016/j.conengprac.2019.104177
9. Erickson, Z., Clever, H.M., Turk, G., Liu, C.K., Kemp, C.C.: Deep Haptic Model Predictive Control for Robot-Assisted Dressing. In: 2018 IEEE International Conference on Robotics and Automation (ICRA). pp. 4437–4444. IEEE, Brisbane, Australia (2018). https://doi.org/10.1109/ICRA.2018.8460656
10. Teramae, T., Noda, T., Morimoto, J.: EMG-Based Model Predictive Control for Physical Human-Robot Interaction: Application for Assist-As-Needed Control. IEEE Robot. Autom. Lett. 3, 210–217 (2018). https://doi.org/10.1109/LRA.2017.2737478
11. Pacheco Quiñones, D., Paterna, M., De Benedictis, C.: Automatic electromechanical perturbator for postural control analysis based on model predictive control. Appl. Sci. 11, 4090 (2021). https://doi.org/10.3390/app11094090
12. Dvir, Z., Paterna, M., Quargnenti, M., Benedictis, C. De, Maffiodo, D., Franco, W.: Linearity and repeatability of postural responses in relation to peak force and impulse of manually delivered perturbations : a preliminary study. Eur. J. Appl. Physiol. 120, 1319–1330 (2020). https://doi.org/10.1007/s00421-020-04364-y
13. Paterna, M., Dvir, Z., De Benedictis, C., Maffiodo, D., Franco, W., Ferraresi, C., Roatta, S.: Center of pressure displacement due to graded controlled perturbations to the trunk in standing subjects: the force–impulse paradigm. Eur. J. Appl. Physiol. 122, 425–435 (2022). https://doi.org/10.1007/s00421-021-04844-9